Numerical prediction of NG spread following intermediate-size LNG spills from ship tankers

M. A. Serag-Eldin
Mechanical Engineering Department, Cairo University, Giza, Egypt

The paper presents a computational model for the numerical prediction of the three-dimensional, time-dependent spread of natural gas (NG) in the atmosphere, following the accidental release of liquefied NG from a ship tanker in the open sea. The model is designed to predict the consequences of liquefied NG spills of intermediate size in which the disturbance to the surrounding atmospheric airflow caused by the effect of the NG release is comparable in magnitude to the one introduced by the tanker's obstruction to the flow. It is applied to predict the NG concentrations arising from two different spill sizes, and typical results are presented and discussed. They are demonstrated to be plausible and informative.

Keywords: atmospheric pollution; heavy gas dispersion; liquefied gaseous fuel spills; LNG spills; marine transport hazards

Introduction

Natural gas (NG) is generally transported overseas in the form of liquefied natural gas (LNG), which is a cyrogenic liquid[1] whose boiling point under atmospheric pressure is approximately $-161°C$. It is carried inside large containers of ship tankers at atmospheric pressure and cooled continuously throughout its voyage in order to keep it from evaporating.

In the event of an accident to an LNG carrier, it is likely that one or more of its containers will fracture, with subsequent spillage of the cryogenic liquid overboard. The LNG liquid, being lighter than seawater but heavier than air, will eventually float over the surrounding water surface and expand outward while simultaneously evaporating into the atmosphere until all of the LNG pool has evaporated. The evaporated LNG (now NG) mixes with the neighboring atmospheric air to create a time-dependent, nonuniform mixture of air and NG. This mixture is flammable within the flammability limits of NG in air, thus introducing serious fire hazards.

Hence, the computation of the concentration of NG in air following an LNG spill is desirable for predicting the propagation of the hazardous region in both space and time. The results may be employed to decide beforehand on conventional emergency measures to be taken in the event of an accident (e.g., to keep nearby traffic out of the predicted hazardous zones). Moreover, the numerical creation of the scenario of events following a spill could assist the development of new methods for reducing hazards (e.g., by examining the feasibility of injecting flame retardants right after the spill, and of incinerating the remaining cargo of a disabled ship in remote cascade burners).[2] The results may also be employed to issue precautionary measures and to check and update current safety regulations, such as minimum allowable distance to be kept between an LNG tanker and a neighboring vessel in normal traffic. They are also obviously useful for conducting fire risk analysis.

However, the computation of the concentration field is complicated due to the following characteristics:

(1) The processes involved are three-dimensional and time-dependent.
(2) Reliable predictions require mathematical models comprising elliptic, partial differential, and nonlinear equations, some of which are strongly coupled.
(3) A wide spectrum of time and length scales has to be considered.
(4) The processes occur in the open atmosphere, and hence proper atmospheric simulation is required, which must be compatible with the turbulence model employed.
(5) The continuously developing LNG pool leads to continuously changing boundary conditions which vary in space and time.
(6) Models are required for the liquid and gaseous states of NG and for the interaction between them.

The present model is concerned with intermediate LNG spills, whose size is defined to be such that the spill causes a disturbance to the surrounding atmospheric flow comparable in magnitude to the one caused by the obstruction of the flow introduced by the presence of the tanker's body. This implies that, for intermediate-sized spills, modeling approximations which may be introduced when the spill is very large or very small are not justified. Very large spills are defined to be large enough for the disturbance to the atmospheric flow introduced by the release of the LNG to overshadow the disturbance due to the presence of the ship's hull; very small spills are defined to be small enough that their disturbance to the atmospheric flow is secondary to the effect of the tanker's body obstruction to the flow.

The present computational model could also be applied to predict small-sized spills; however, it would not be as efficient as models designed specifically for that purpose.[3] Theoretically speaking, the present model could also be employed to predict large-sized spills; however, the computational effort required might be prohibitive, and considerably more than required by the special model presented elsewhere for large spills.[4]

The computational model presented here comprises two distinct models: a gaseous phase model for the NG-air mixture, and a liquid-phase model for the LNG pool. The output of the liquid pool model is input to the gaseous phase model as a boundary condition for the latter, but no feedback is propagated from the gaseous phase to the liquid one. To render the computation of the problem investigated tractable and practical, we developed a special computational model designed to exploit the numerical characteristics of the problem considered. This

Address reprint requests to Professor M. A. Serag-Eldin, Mechanical Engineering Department, Cairo University, Giza, Egypt.
Received 29 May 1987; accepted for publication 21 October 1988

© 1989 Butterworth Publishers

model is presented here together with the results of its application to two sample cases.

NG-air model governing equations

The NG-air model comprises governing differential equations expressing three-dimensional, time-dependent mass conservation of the mixture (continuity) and of the NG species (concentration), momentum balance in three orthogonal directions, and the transport of the kinetic energy of turbulence k and its rate of dissipation ε. The latter two equations are introduced by the adopted k-ε turbulence model.[5]

In the k-ε model the eddy diffusivity μ_t is derived from k and ε according to

$$\mu_t = \rho C_\mu k^2/\varepsilon \tag{1}$$

where ρ is the NG-air mixture density, and C_μ is a turbulence model constant whose value is displayed with the other model constants C_1, C_2, σ_k, σ_ε, and σ_c in Table 1. The effective viscosity μ_{eff} is thus

$$\mu_{\text{eff}} = \mu + \mu_t \tag{2}$$

where μ is the molecular viscosity of the NG-air mixture.

Assuming the seawater surface to coincide with a horizontal plane, we use the Cartesian coordinate system, where the x denotes the direction of the free atmospheric wind, y denotes the horizontal normal to x, and z denotes the vertical direction measured upward from the seawater surface, as sketched in Figure 1.

All governing differential equations for the gaseous phase may be cast in the following concise form:

$$\frac{\partial(\rho\phi)}{\partial t}+\frac{\partial(\rho u\phi)}{\partial x}+\frac{\partial(\rho v\phi)}{\partial y}+\frac{\partial(\rho w\phi)}{\partial z} = \frac{\partial(\Gamma_\phi\,\partial\phi/\partial x)}{\partial x}+\frac{\partial(\Gamma_\phi\,\partial\phi/\partial y)}{\partial y}+\frac{\partial(\Gamma_\phi\,\partial\phi/\partial z)}{\partial z}+S_\phi \tag{3}$$

where t denotes time, u, v, and w denote the velocity components in the x, y, and z directions, respectively, ϕ denotes any dependent variable, Γ_ϕ denotes the diffusion coefficient of ϕ, and S_ϕ denotes the source term of ϕ.

Table 2 gives ϕ, Γ_ϕ, and S_ϕ for each variable ϕ, with $\phi=1$ expressing the continuity equation; p denotes the pressure difference between the local static pressure and the hydrostatic pressure $-\rho gz$, c is the NG concentration in the mixture (mass fraction), g is the gravitational acceleration, and the subscript a pertains to the undisturbed atmospheric conditions and properties.

Since the Mach number of the flow is always low, the mixture density ρ is determined from the equation of state with a uniform value of the atmospheric pressure p_a:

$$\rho = p_a/RT \tag{4}$$

where the mixture gas constant R is determined from c, the NG gas constant R_{NG}, and the air gas constant R_a:

$$R = (1-c)R_a + cR_{\text{NG}} \tag{5}$$

The mixture temperature T is evaluated from c, the LNG

Table 1 Turbulence model constants

κ	C_μ	C_1	C_2	σ_k	σ_ε	σ_c
0.435	0.09	1.44	1.92	1.0	1.3	0.7

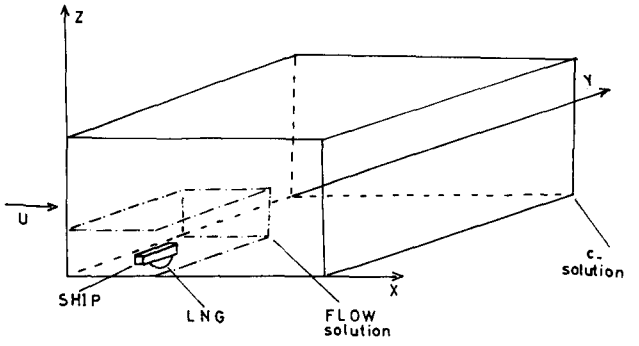

Figure 1 Integration domains for intermediate spills model

Notation

c	Concentration (mass fraction) of NG
C_1, C_2, C_μ	Turbulence model constants
g	Acceleration of gravity
G_b	Buoyant production term
h_l	Height of LNG pool
k	Kinetic energy of turbulence
$\dot{m}_e$	LNG evaporation rate
p	Pressure
R	Gas constant
Ri	Richardson number
R_l	LNG pool radius
S_ϕ	Source term of ϕ
t	Time
T	Temperature
U	Atmospheric velocity
u, v, w	Cartesian velocity components
$\dot{V}_s$	LNG volumetric spill rate
$V_{l,i}$	LNG initial pool volume
x, y, z	Cartesian coordinates (Figure 1)
z_0	Aerodynamic roughness of sea surface
α	Angle subtended by LNG pool
β	LNG pool model constant
Δx, Δz	Grid spacing in x, z directions
ε	Dissipation rate of k
Γ	Diffusion coefficient
ϕ	Any dependent variable
κ	Von Karman's constant
μ	Molecular viscosity
μ_t	Eddy viscosity
μ_{eff}	Effective viscosity
ρ	Mass density
σ_k, σ_ε, σ_c	Turbulence model constants
τ_s	Surface shear stress

Subscripts

a	Pertaining to undisturbed air
l	Pertaining to LNG
max	Maximum value, at maximum extent
NG	Pertaining to NG
w	Pertaining to water
ϕ	Pertaining to ϕ

Superscripts

′	Fluctuating component
—	Time average

Table 2 Gaseous phase model variables

Equation	ϕ	Γ_ϕ	S_ϕ
Continuity	1	0	0
Concentration	c	μ_{eff}/σ_c	0
x momentum	u	μ_{eff}	$-\partial p/\partial x+\partial(\mu_{eff}\,\partial u/\partial x)/\partial x+\partial(\mu_{eff}\,\partial v/\partial x)/\partial y+\partial(\mu_{eff}\,\partial w/\partial x)/\partial z$
y momentum	v	μ_{eff}	$-\partial p/\partial y+\partial(\mu_{eff}\,\partial u/\partial y)/\partial x+\partial(\mu_{eff}\,\partial v/\partial y)/\partial y+\partial(\mu_{eff}\,\partial w/\partial y)/\partial z$
z momentum	w	μ_{eff}	$-\partial p/\partial z-(\rho-\rho_a)g+\partial(\mu_{eff}\,\partial u/\partial z)/\partial x+\partial(\mu_{eff}\,\partial v/\partial z)/\partial y+\partial(\mu_{eff}\,\partial w/\partial z)/\partial z$
k transport	k	μ_{eff}/σ_k	$G_k{}^{*}+G_b{}^{**}-\rho\varepsilon$
ε transport	ε	$\mu_{eff}/\sigma_\varepsilon$	$C_1\varepsilon/k(G_k+G_b)-C_2\rho\varepsilon^2/k$

$$^{*}\,G_k=\mu_t\left\{2\left[\left(\frac{\partial u}{\partial x}\right)^2+\left(\frac{\partial v}{\partial y}\right)^2+\left(\frac{\partial w}{\partial z}\right)^2\right]+\left(\frac{\partial u}{\partial y}+\frac{\partial v}{\partial x}\right)^2+\left(\frac{\partial u}{\partial z}+\frac{\partial w}{\partial x}\right)^2+\left(\frac{\partial v}{\partial z}+\frac{\partial w}{\partial y}\right)^2\right\}$$

$$^{**}\,G_b=\frac{g\mu_t}{\sigma_c}\left(\frac{\partial c}{\partial z}\right)\left\{\frac{R_a-R_{NG}}{R}+\frac{T_a-T_{LNG}}{T}\right\}$$

evaporation temperature T_{LNG}, and the undisturbed atmospheric air temperature T_a:

$$T=(1-c)T_a+cT_{LNG} \tag{6}$$

Equation 6 is an outcome of assuming uniform values of specific heat and adiabatic mixing, and neglecting viscous dissipation heating, pressure, and radiation source terms in the energy equation. By these assumptions the dimensionless form of the temperature energy equation and its boundary conditions become identical to those for c, hence the linear dependence of T on c only.

The buoyant production of turbulent kinetic energy per unit volume of the mixture $G_b=-g\overline{\rho' w'}$ is given at the bottom of Table 2. It is deduced from Equations 4 to 6 after differentiation, and employing $-\overline{c'w'}=(\mu_t/\rho\sigma_c)(\partial c/\partial z)$.

The integration domain displays the following types of boundaries.

Bottom boundary

The bottom boundary is $z=0$ and corresponds to the entire sea surface except the area occupied by the tanker. This also includes the area covered by the LNG pool, where the pool thickness is neglected. For all variables except c, solid wall boundary conditions are imposed at this boundary with the aid of "wall functions."[6,7] For c the boundary conditions are generally zero diffusion (i.e., $\partial c/\partial z=0$) except where and when the LNG pool releases NG in the atmosphere, in which case the boundary condition gives the local rate of NG mass released.

Free atmospheric flow boundaries

Free atmospheric flow boundaries generally comprise the inflow boundary $x=0$, the lateral boundaries $y=0$ and $y=y_{max}$, and the upper boundary $z=z_{max}$, where the subscript max denotes the maximum extent of the integration domain. However, if symmetry conditions are present over the y plane passing through the midsection of the hull, then for obvious reasons of economy the $y=0$ boundary is placed at this section and displays symmetrical boundary conditions. The free atmospheric flow boundaries are located far enough upstream or above the tanker that the flow there may be assumed to conform to the free atmospheric flow. The folllowing set of atmospheric boundary conditions is imposed at the $x=0$ boundary, with similar ones imposed at the other atmospheric flow boundaries:

$$u=\frac{1}{\kappa}\left(\frac{\tau_s}{\rho_a}\right)^{1/2}\ln\left(\frac{z}{z_0}\right) \tag{7a}$$

$$v=w=c=0 \tag{7b}$$

$$k=\frac{\tau_s}{\rho_a C_\mu^{1/2}} \qquad \varepsilon=\frac{(\tau_s/\rho_a)^{3/2}}{\kappa z} \tag{7c}$$

where τ_s gives the prevailing value of the surface stress at $z=0$, ρ_a is the mass density of air, z_0 is the aerodynamic roughness, and κ is Von Karman's constant (Table 1). It is obvious that τ_s is one of the parameters of the problem. However, it is unusual to know its value explicitly; instead it is customary[8] to specify the atmospheric wind velocity profile in the form of a power law as follows:

$$U/U_{max}=(z/z_{max})^{1/n} \tag{8}$$

where $1/n$ is the power-law index, and U and U_{max} denote the atmospheric wind velocity at height z and z_{max}, respectively. In this case the value of τ_s is determined from the following relation to yield a logarithmic velocity profile producing the same inflow mass flux:[9]

$$\tau_s=\rho_a\left\{\frac{n\kappa U_{max}}{(n+1)\ln(z_{max}/z_0)-(n+1)}\right\}^2 \tag{9}$$

The set of atmospheric conditions presented here simulate the atmospheric surface layer flow fairly closely, particularly for near-neutral stability conditions. Moreover, this set is compatible with the turbulence model employed; i.e., they themselves are the solution of the NG-air model equations in the absence of a disturbance to the atmospheric flow (the tanker and NG in this case), which is what we should expect. Recently,[10] a method was suggested for extending the present turbulence model and atmospheric boundary conditions to moderately stable and unstable flows. However, for strongly stable or unstable flows it may be more appropriate to employ a different model of turbulence and deduce another realizable and compatible set of boundary conditions.

Outflow boundary

The outflow boundary is the far downstream $x=$constant boundary; it is located far enough downstream from the LNG pool that the flow there may be assumed to be fully developed. Thus, zero x-direction gradients of the dependent variables are imposed at this boundary in addition to a uniform exit value of p.

Tanker boundaries

Tanker boundaries constitute the outer surface of the tanker and are solid wall boundaries. They are thus treated accordingly,

with the aid of "wall functions." Zero diffusion of c is assumed at these boundaries, although this may be changed according to the problem. Whatever the direction of the atmospheric wind with respect to the tanker hull axis, it is always recommended that while using the proposed upwind differencing scheme the direction of the x axis should be aligned with the direction of the atmospheric wind, even though this means that the hull boundaries would have to be expressed by a ragged profile formed of orthogonal control-volume surfaces when the atmospheric flow direction is not normal to it. This is done in order to avoid unacceptably large values of numerical diffusion in regions remote from the ship where the physical diffusion is relatively low close to the surface, the grid spacing is large, and the magnitude of the velocities is high, all of which contribute to high levels of numerical diffusion if the angle subtended between the local velocity vector and the closest grid line direction is not very small. With the present recommendation the numerical diffusion levels should generally be low since the flow follows the x direction closely in the regions remote from the tanker, and in the neighborhood of the tanker where the flow inclination is a maximum, the physical diffusion is high, the grid spacing is smallest, and the magnitude of the local velocities is often small (particularly in the recirculation region). Alternatively, if more accuracy is needed at the expense of additional computational costs, then the x or y directions could be aligned with the direction of the hull axis in order to express the hull geometry more accurately; the atmospheric flow should be resolved into the x and y directions and introduced through the x and y inflow boundaries; and a skew[11] or vector[12] upstream differencing scheme should be adopted in order to reduce numerical diffusion.

LNG pool model

A gravity spread model is presented here for the LNG liquid pool, which is based on a balance between gravity forces and pool inertia, assuming that the pool forms a segment of a cylinder subtending a constant angle α (radians) whose height and radius are changing with time. In most cases, the pool cross section may be assumed to form a semicircle whose straight edge is attached to one side of the tanker's hull, for which case $\alpha=\pi$.

Gravity spread models which yield analytical solutions have been presented elsewhere.[13,14] They are subject to somewhat restrictive conditions in order to yield analytic solutions. A similar model, but including the term expressing the gain in momentum of the spilt LNG and subject to more general and realistic conditions, is presented here, albeit at the price of requiring numerical integration by the Runge-Kutta method.

If we assume the liquid pool to form a cylinder of height h_l and radius R_l at any instant of time t, a momentum balance yields

$$\beta\left(1-\frac{\rho_l}{\rho_w}\right)R_l g h_l^2 = h_l R_l^2 \frac{d^2R_l}{dt^2} + \frac{2}{\alpha}\dot{V}_s \frac{dR_l}{dt} \tag{10}$$

where $\dot{V}_s$ is the volumetric rate of LNG split per unit time, ρ_l and ρ_w are the fluid densities of LNG and water, respectively, and β is a correction factor to account for the fact that not all the fluid is flowing with leading-edge velocity. Here $\beta=2$.[13]

Mass balance for the liquid pool yields

$$h_l = \frac{2}{\alpha R^2}\left[V_{l,i} + \int_0^t \dot{V}_s\,dt - \frac{\alpha}{2\rho_l}\int_0^t \dot{m}_e R_l^2\,dt\right] \tag{11}$$

where $V_{l,i}$ is the initial pool volume at the start of spill $t=0$, and $\dot{m}_e$ is the evaporation rate of LNG per unit area of pool surface. An empirical value[14] of $\dot{m}_e=0.045\,\mathrm{kg\,m^{-2}\,s^{-1}}$ is used. Equations 10 and 11 are subject to the initial conditions

$$R_l = R_{l,i} \qquad \frac{dR_l}{dt}=0 \qquad \text{at } t=0 \tag{12a}$$

$$h_l = \frac{2V_{l,i}}{\alpha R_{l,i}^2} \qquad \text{at } t=0 \tag{12b}$$

where $R_{l,i}$ designates the initial LNG pool radius. In addition, $\dot{V}_s$ is a parameter which has to be specified at all times.

Solution of model equations

Solution procedure

An upwind differencing discretization scheme is employed which is conservative and adopts a finite-difference control-volume-based approach. The equations are solved with the aid of the SIMPLE algorithm.[15,16] The solution procedure is similar to the one employed for very large spills and reported in detail elsewhere.[4]

Special features

For any spill of finite size, it is expected that in regions far from the spill the concentration of NG in air will be small enough for buoyancy terms to be neglected. Thus in these regions the effect of the concentration field on the flow field may be justifiably neglected.

Moreover, after a sufficient time following the evaporation of the LNG pool, the convection and diffusion processes would inevitably reduce the concentration of NG in the whole atmosphere to a level below which the buoyancy forces are no longer influential. If we define a cell Richardson number $\mathrm{Ri}\equiv(\rho-\rho_a)\,\Delta x g/\rho u^2$, where Δx is the x-direction grid spacing, and adopt a critical value of $\mathrm{Ri}=0.05$ below which buoyancy source terms may be removed from the discretization equations; then, as an example, for the demonstration cases presented later this value of Ri corresponds to a value of $c\approx 0.10$. This value of c is still considerably above the lower flammability limits of NG in air, and hence the computation of the concentration field is still required. For finer grids, lighter LNG compositions, or higher velocities, the critical value of c at which uncoupling of the computations occurs is higher, and vice versa.

To reduce computational effort, we want to uncouple the flow field from the concentration field whenever this is justified. This is achieved here by means of the following two special features of the present computational algorithm.

(1) The concentration field integration domain is chosen to cover the whole space where the concentration of NG in air is likely to be of practical importance. This field may also expand with time as the need arises. The flow field integration domain is chosen to occupy only the portion of the concentration field where the concentration of NG in air is likely to be high enough that buoyancy forces are important (Figure 1). In the space covered by the concentration field integration domain, but not by the flow field domain, the flow field is assumed to correspond to that of the free atmospheric flow. This feature allows fewer computations of the flow field in much of the space, and it also curbs the numerical instabilities introduced by the solution of the flow equations in the highly nonuniform expanding grid at the remote sections.

(2) After a sufficient time following the evaporation of all the spilt LNG, such that the concentration of NG in air throughout the whole field is small enough for buoyancy terms to be negligible, the coupling of the flow field to the concentration field is gradually removed (over 20 steps typically), and finally

the flow field is fixed for all subsequent computations of the concentration field. A smooth transition is achieved primarily through the gradual replacement of increasing proportions of ρ calculated from Equation 4 by ρ_a, thus gradually eliminating the buoyancy terms. Fixing the flow field results in saving much computation time, not only due to fewer computations for the flow field (u, v, w, k, and ε fields), but also because, after fixing the flow field, much longer time steps may be employed than would otherwise have been allowable by the coupled nonlinear equations of the flow field.

Discussion of computational model

The mathematical model presented here involves a fair amount of approximations and assumptions, which inevitably must affect the accuracy of the predictions. Almost all the models presented here may be improved or replaced by more sophisticated ones which are readily available in the literature. Thus, for example, a Reynolds stress model could be adopted instead of the two-equation k-ε turbulence model used here; a more detailed liquid pool model could be employed, which features partial differential equations,[17,18] the finite thickness of the pool could be taken into account, and an analysis of the heat and mass transfer at the pool surface could be performed to determine the evaporation rate of LNG rather than the use of the uniform empirical value; the adiabatic assumption could also be removed, heat transfer at the water surface introduced, and a separate energy equation solved; variation of the specific heat with temperature and concentration could be included, as could a more sophisticated equation of state. It is also possible to adopt a more advanced differencing scheme in order to reduce discretization errors, as mentioned earlier.

However, all the above improvements are at the expense of increased computational effort, in a problem which is already computationally demanding, and for which a specially designed numerical solution procedure was contrived in order to reduce those requirements and render the numerical predictions practical.

Moreover, the practical applications in view do not warrant high accuracy at the expense of high cost; this is because spills are accidental, and thus it is not possible to know a priori under which set of conditions a real spill will occur, and thus an infinite number of combinations of parameters is possible. Hence, it is expected that the computational model will be chiefly employed to predict a discrete number of cases, which will be used to provide average quantities or to serve as interpolating results for other cases. Averaging or interpolating in a highly nonlinear phenomenon such as the present one introduces a fair amount of error regardless of the precision of simulating any set of conditions. A larger tolerance for inaccuracy must therefore be accepted from models for the present applications than for those for other applications in which the computational requirements are considerably less or the accuracy requirements are more stringent.

The present model is chosen to be refined enough to provide the level of reliability demanded by the applications it is expected to be used for, yet not overrefined so that the computational requirements would not be excessive.

Demonstration cases

The computational model is employed here to predict the development of the concentration fields resulting from two different LNG spills from a ship tanker. One of these features a total volume of $100\,m^3$ spilt at a uniform rate of $10\,m^3/s$, whereas the other involves a total volume of $1000\,m^3$ spilt at a uniform rate of $100\,m^3/s$. Both spills share all the other parameters, including:

Tanker dimensions (length × breadth × height above water)	250 m × 20 m × 9 m
Origin of spill	Center of leeward side
α for LNG pool	π (radians)
Atmospheric wind velocity	4.3 m/s at 2 m height
Power-law index ($1/n$)	0.10
z_0 for open sea	10^{-3} m

Some of the solution details for the 1000-m^3 spill are as follows:

Integration domains in x, y, z directions, respectively:

Flow field	(1700)(1400)(80) m
c field	(15,000)(4500)(190) m

Number of grid nodes in x, y, z directions, respectively:

Flow field	(32)(23)(17)
c field	(38)(26)(20)
Smallest/largest Δx for flow field	4 m/200 m
Smallest/largest Δz for flow field	0.2 m/17 m

The time step during the LNG pool expansion and evaporation period was as low as 0.3 s. This was necessary for both numerical stability and accuracy reasons (in order to capture the rapidly changing boundary conditions). After the evaporation of the LNG pool, the time step was slowly increased until the decoupling of the momentum field from the concentration field at low values of Ri was performed. The time steps were then increased fairly rapidly to reach approximately 7 s toward the end of the solution period (600 s).

Demonstration results

Figures 2 to 5 present selected concentration contour lines for the 100-m^3 spill, and Figures 6 to 9 reveal the contour lines for the 1000-m^3 spill. The contour lines are presented for $c=0.001, 0.01, 0.05, 0.1, 0.2$, and 0.5 at $z=0.2$ m, 0.7 m, 1.45 m, 4 m, and 13 m above the seawater surface and at different time steps following the start of the spill. The absence of any of the contour lines at a given z plane indicates the absence of that concentration level at this plane, whereas the absence of a horizontal z plane from among the selected z planes indicates either the absence of the $c=0.01$ line at this height or practically the same profile as a previously displayed one. The heavy solid line plotted at $x=96$ m for $z<9$ m represents the leeward side of the ship's hull.

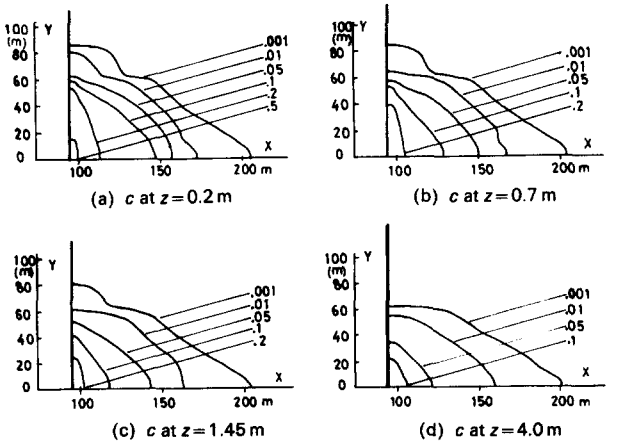

(a) c at $z=0.2$ m (b) c at $z=0.7$ m

(c) c at $z=1.45$ m (d) c at $z=4.0$ m

Figure 2 Concentration contours 30 s after 100-m^3 spill

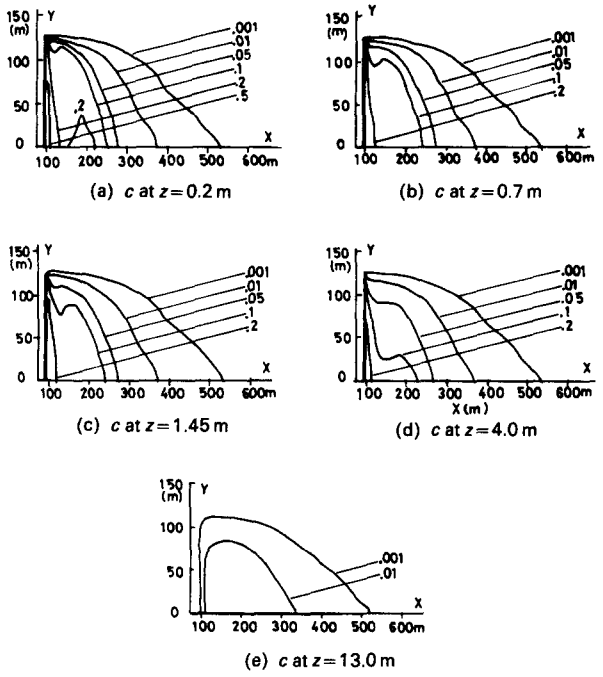

Figure 3 Concentration contours 80 s after 100-m³ spill

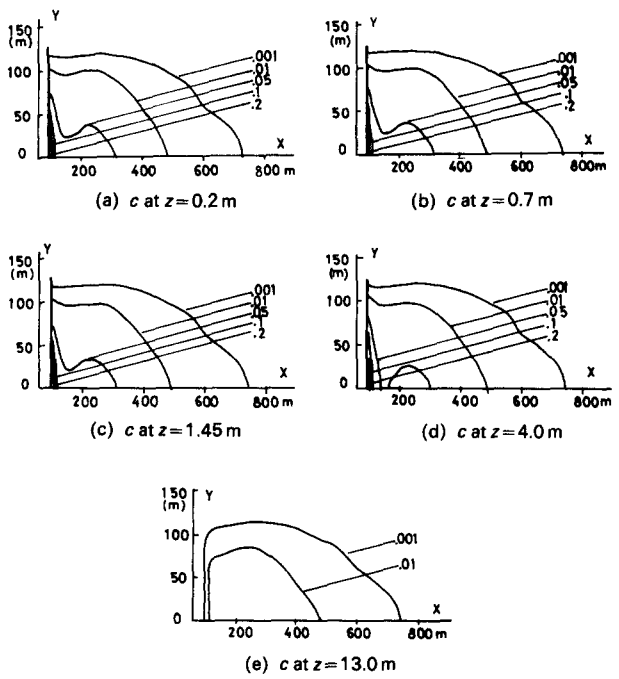

Figure 4 Concentration contours 110 s after 100-m³ spill

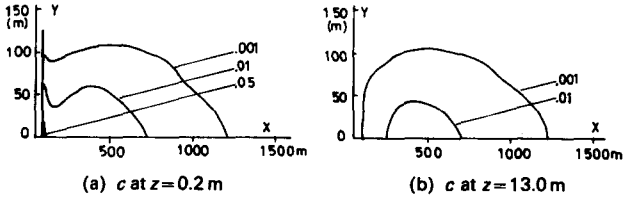

Figure 5 Concentration contours 170 s after 100-m³ spill

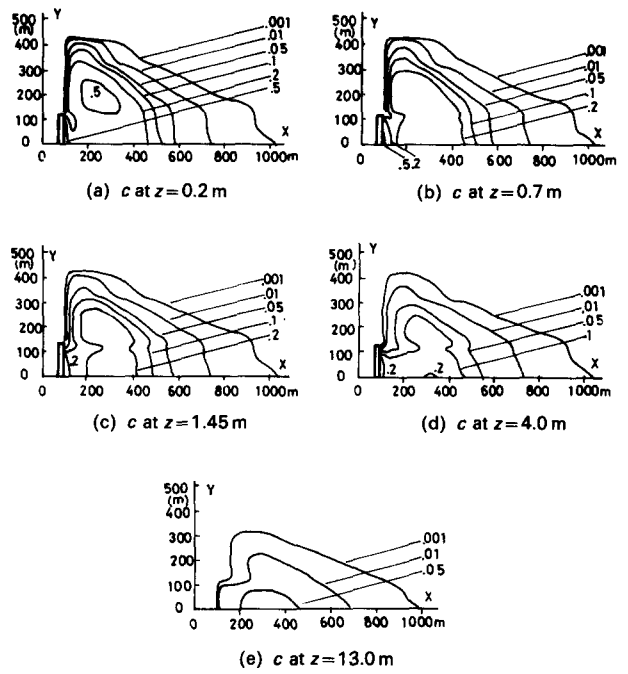

Figure 6 Concentration contours 112 s after 1000-m³ spill

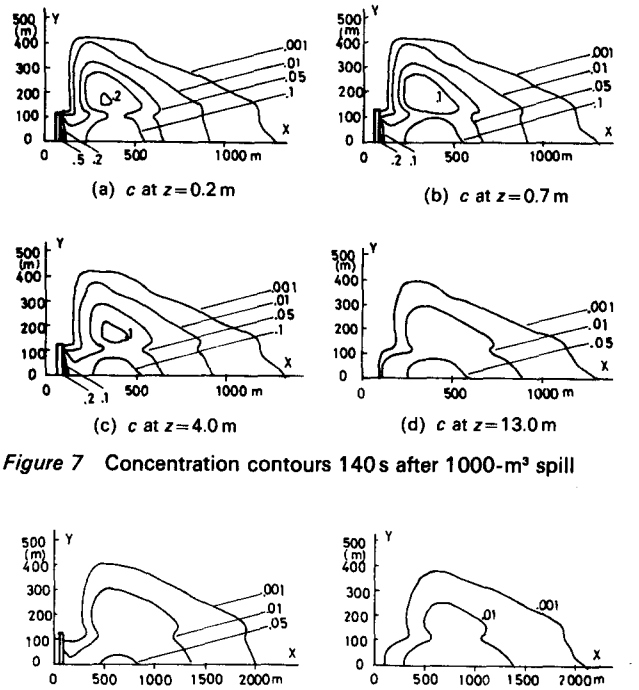

Figure 7 Concentration contours 140 s after 1000-m³ spill

Figure 8 Concentration contours 220 s after 1000-m³ spill

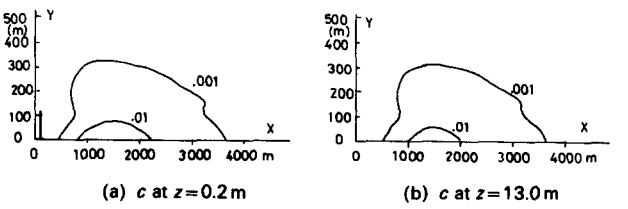

Figure 9 Concentration contours 390 s after 1000-m³ spill

Table 3 Hazardous range for each case

Case of (m^3)	$c=0.01$ max. extent in			$c=0.01$ max. duration		LNG pool max.	
	x (m)	y (m)	z (m)	Close to ship (s)	Everywhere (s)	Radius (m)	Duration (s)
100	900	250	32	280	290	121	75
1000	2400	800	45	290	550	328	111

The $c=0.01$ contour lines may be considered to contain the region exposed to fire hazards. This is based on the knowledge that the lower flammability limit of NG in air is about 5% and that peak-to-average concentration ratios of 3:1 are not uncommon for such flows.[19,20] The remaining factors are to guard against spikes in the peak-to-average ratios and the smearing of the predicted concentration peaks introduced by the computational technique.

Table 3 presents the predicted extent and duration of the flammable NG-air mixture for each case. It also reveals the duration of the LNG pool evaporation and the maximum radius of the LNG pool.

Discussion of results

Inspection of the results reveals that they are consistent, plausible, and interesting. As an example, the following observations are made.

(1) At the onset of the spill and for a short time after, the concentration profiles are smooth and their peak is observed to lie on the centerline; however, as the concentration field builds up, the c profiles in the region of high concentration of NG become less smooth and peaks appear away from the center line. This phenomenon is only observed in regions of high concentration and is much more pronounced for larger spills, which implies that it is caused by the concentration of NG. It is attributed to the rapidly changing flow pattern due to the rapid change in the mass input from the pool, and to the rapidly changing buoyancy force with time as a result of the fairly rapid buildup and decay of concentrations. For LNG-air mixtures it is known[21] that the density of the mixture is less than that of air for small concentrations and larger than that of air for large concentrations, thus causing the local buoyancy force sign to generally go through three phases: positive, negative, and positive tending to zero.

(2) Examining some of the profiles reveals that after a sufficient time, the concentration field is roughly split into two distinct fields: one attached to the wake on the leeward side of the tanker, and the other convected downstream by means of the forward flow far from the tanker. For the smaller spill, as is apparent from Table 3, the duration of the NG concentrations above 1% which are attached to the tanker is approximately equal to their duration far downstream. However, for the larger spill the volume of the NG convected downstream is considerably larger than that retained in the wake of the ship, and hence the duration of concentration in excess of 1% is considerably longer far downstream.

(3) Although the 1000-m^3 spill involves 10 times the volume of the 100-m^3 spill, the increase in the LNG evaporation time (pool duration) for the larger spill is only 48%. This is due to the considerably larger pool area for the large spill (whose radius is 328 m) than for the small spill (whose radius is 121 m), causing a much larger total LNG evaporation rate for the larger spill.

(4) The extent of the $c=0.01$ contour line in the x and y directions for the 1000-m^3 spill is approximately three times the corresponding extent for the 100-m^3 spill, whereas the extent in the z direction for the larger spill is only 40% greater than for the smaller spill. This is probably due to the larger pool radius for the larger spill, causing the NG to spread over a larger area; however, it could also have been influenced by the larger total negative buoyancy force for the larger spill tending to stop the flow from moving upward and forcing it horizontally during the duration of periods of large levels of c.

(5) The concentration profiles differ greatly with size of spill; hence extrapolation of results to larger spills should be avoided, and interpolation should be undertaken with care.

Summary and conclusion

The paper presents a computational model for predicting the complicated phenomena following intermediate-sized LNG spills. Even though the model employs three-dimensional, time-dependent conservation equations, its computational requirements are not excessive, due to its ability to exploit two special features of the problem. Results of computations performed are presented, which demonstrate the feasibility of performing such predictions. They also reveal how effective they could be for conducting risk analysis and examining preventive and emergency measures, as well as for gaining insight into these intricate phenomena.

References

1 Tiratsoo, E. N. *Natural Gas*, 3rd ed. Gulf Publishing, Houston, 1979

2 Liquified gaseous fuels safety and environmental control assessment program: third status report, March 1982, Pacific Northwest Lab. Battelle Memorial Institute

3 Serag-Eldin, M. A. Spread of NG following a small LNG spill from a ship-tanker. *Proc. 4th Int. Conf. Num. Methods in Thermal Problems*, Swansea, Part 2, 1985, pp. 1563–1577

4 Serag-Eldin, M. A. Computation of NG spread following very large LNG spills from shiptankers. *Appl. Math. Modelling* 1988, **12**, 238–248

5 Launder, B. E. and Spalding, D. B. The numerical computation of turbulent flows. *Comput. Meth. Appl. Mech. Eng.* 1974, **3**, 269–289

6 Launder, B. E. and Spalding, D. B. *Mathematical Models of Turbulence*. Academic Press, 1972

7 Patankar, S. V. and Spalding, D. B. *Heat and Mass Transfer in Boundary Layers*. Intertext Books, 1970

8 Cermak, J. E. Applications of fluid mechanics to wind engineering —a Freeman scholar lecture. *J. Fluids Eng. Trans. ASME* March 1975, **97**, 9–38

9 Serag-Eldin, M. A. Computation of the atmospheric surface-layer flow over a wide, inclined, backward facing step. IBM CSC Techn. Report No. 007, October 1984

10 Abou-Arab, T. W. and Serag-Eldin, M. A. Turbulence modelling and simulation of atmospheric boundary layers. To be published at *Int. Symp. Modeling Environmental Flow*, ASME Winter Annual Meeting, Dec. 1987, FED, **59** 25–30

11 Raithby, G. D. Skew upstream differencing schemes for problems involving fluid flow. *Comput. Meth. Appl. Mech. Eng.* 1976, **9**, 153–164

12 Lillington, J. N. A vector upstream differencing scheme for problems in fluid flow involving significant source terms in steady-state linear systems. *Int. J. Num. Meth. Fluids* 1981, **1**, 3–16

13 Briscoe, F. and Shaw, P. Spread and evaporation of liquid. *Prog. Energy Comb. Sci.* 1980, **6**, 127–140

14 Opschoor, G. Investigations into the spreading and evaporation of LNG spilled on water. *Cryogenics* Nov. 1977, 629–633

15 Caretto, L. S., Gosman, A. D., Patankar, S. V., and Spalding, D. B. Two calculation procedures for steady three-dimensional flow with recirculation. *Proc. 3rd Int. Conf. Num. Methods in Fluid Mechanics*, **II**, 1973, pp. 60–68

16 Patankar, S. V. *Numerical Heat Transfer and Fluid Flow*. Hemisphere, 1980

17 Brandeis, J. and Kansa, E. J. Numerical simulation of liquefied fuel spills: I. Instantaneous release into a confined area. *Int. J. Num. Meth. Fluids* 1983, **3**, 333–345

18 Brandeis, J. and Ermak, D. L. Numerical simulation of liquefied fuel spills: II. Instantaneous and continuous LNG spills on an unconfined water surface. *Int. J. Num. Meth. Fluids* 1983, **3**, 347–361

19 Koopman, R. P., Cederwall, R. T., Ermak, D. L., Goldwire, H. C., Hogan, W. J., McClure, J. W., McRae, T. G., Morgan, D. L., Rodean, H. C., and Shinn, J. H. Analysis of Burro series 40m3 LNG spill experiments. *J. Hazardous Materials* 1982, **6**, 43–83

20 Drake, E. M. and Putnam, A. A. Vapor dispersion from spills of LNG on land. *Adv. in Cryog. Eng.* 1975, **20**, 134–142

21 Meroney, R. N., Cermak, J. E., and Neff, D. E. Dispersion of vapor from LNG spills—simulation in a meteorological wind tunnel. *AMS Third Symposium on Atmospheric Turbulence, Diffusion and Air Quality*, Raleigh, 1976, 1–4